Silicon Heterojunction Solar Cells with MoO_x Hole-Selective Layer by Hot Wire Oxidation–Sublimation Deposition

Li, Fengchao; Zhou, Yurong; Yang, Ying; Dong, Gangqiang; Zhou, Yuqin; Liu, Fengzhen; Yu, Donghong

Published in:
Solar RRL

DOI (link to publication from Publisher):
10.1002/solr.201900514

Publication date:
2020

Document Version
Accepted author manuscript, peer reviewed version

Silicon heterojunction solar cells with MoO_x hole selective layer by hot wire oxidation-sublimation deposition

Fengchao Li[1,2,3], Yurong Zhou[1]*, Ying Yang[1], Gangqiang Dong[1], Yuqin Zhou[1], Fengzhen Liu[1,2]*, Donghong Yu[3,4]

1 . Center of Materials Science and Optoelectronics Engineering & College of Materials Science and Opto-Electronic Technology, University of Chinese Academy of Sciences, 100049, Beijing, China
E-mail Y. Zhou: zhouyurong@ucas.ac.cn
E-mail F. Liu: liufz@ucas.ac.cn

2. Sino-Danish College, University of Chinese Academy of Sciences, 100190, Beijing, China

3. Department of Chemistry and Bioscience, Aalborg University, DK-9220, Aalborg, Denmark

4. Sino-Danish Center for Education and Research, Aarhus, DK-8000, Denmark, DK-8000, Denmark

Abstract

In this article, a novel hot wire oxidation-sublimation deposition (HWOSD) technique, as an optional technology, was developed to prepare molybdenum oxide (MoO_x) thin films. Silicon heterojunction (SHJ) solar cells with the HWOSD MoO_x as a hole selective transport layer (HSL) were fabricated. A power conversion efficiency up to 21.10% was achieved on a champion SHJ solar cell using a 14nm MoO_x layer as the HSL. Dark current density-voltage-temperature (*J-V-T*) characteristics of the SHJ solar cell were measured at the temperatures from 200K to 380K. Transport processes including thermionic emission of electrons over the potential barrier and quantum assisted tunneling of holes through the gap states in the MoO_x layer were used to fitting the J-V curves of the MoO_x/n c-Si heterojunction. The investigation of the transport mechanisms provides us a better understanding of the characteristics of the novel SHJ solar cells and it is helpful for us to fully demonstrate the potential of such kind of solar cells in the future.

Keywords: Hot wire oxidation-sublimation deposition, Molybdenum oxide thin film,

This article has been accepted for publication and undergone full peer review but has not been through the copyediting, typesetting, pagination and proofreading process, which may lead to differences between this version and the Version of Record. Please cite this article as doi: 10.1002/solr.201900514

Hole selective transport layer, Silicon heterojunction solar cell, Transport mechanisms

1. Introduction

More and more attention has been paid to the novel silicon heterojunction (SHJ) solar cells by making use of metal oxides to replace the conventional doped hydrogenated amorphous Si (a-Si:H) thin films as the carrier selective transport layers [1, 2-4]. Due to the wide band-gap nature, optional work functions and relatively simple fabrication techniques related to the metal oxides, the novel SHJ solar cells show great potential to further improve the efficiency and reduce the cost of c-Si based solar cells[2, 5]. Difference between work functions of the metal oxides and Fermi level of the c-Si leads to a large energy band bending of the c-Si near the interface, which allows only one type of carriers to pass through and inhibits carrier recombination at the interface[6]. Some metal oxides with high work functions, such as MoO_x [2, 3], VO_x [7], WO_x [8], NiO_x [9, 10] and CuO_x [11, 12], can provide a good hole selective transport when they form heterocontacts with c-Si. Similarly, some metal oxides with low work functions, e.g. TiO_x [9, 13], MgO_x [14, 15] and ZnO[16], can be used as the electron selective transport layers instead of n-type a-Si:H in c-Si solar cells.

Based on such a factor that it is more difficult to obtain high quality p-type a-Si:H than n-type a-Si:H, people are more eager to find a suitable substitute for p-type a-Si:H in SHJ solar cells. In recent years, remarkable achievements have been made on the SHJ solar cells using molybdenum oxide (MoO_x) with wide band-gap (3.0-3.3 eV) and high work function (>6 eV) as the HSL to replace the p type a-Si:H thin film[4, 17, 18, 19]. Various techniques, such as thermal evaporation[2-4], electron beam evaporation[15, 20], atomic layer deposition[21], sputtering[22] and solution-processed method[5], etc. , are available in preparation of MoO_x thin films. By using thermal evaporated MoO_x thin films as the HSL, silicon heterojunction solar cells with the power conversion efficiencies up to 22.5% were fabricated by Jonas Geissbuhler et al. [2]. Jing Yu et al. [15] prepared the MoO_x films using electron beam evaporation and achieved an efficiency of 14.2% on a plane SHJ solar cell with the structure of MoO_x/n-type c-Si/MgO. A solution-processed method was reported by Jingnan Tong et al. [5] to form the MoO_x layers by spin-coating hydrogen molybdenum bronze solution on crystalline silicon wafer surfaces. The developments of the novel heterojunction solar cells with the MoO_x HSL are very exciting and the efficiency is

expected to be further improved in the future.

To promote the commercialization of the novel SHJ solar cells in the future, a simple and scalable production technique capable of fabricating high quality MoO_x thin films is needed. Different from the methods mentioned above, in this work, we provide a new alternative technique for the fabrication of the MoO_x film. We developed a hot wire oxidation-sublimation deposition (HWOSD) technique to fabricate amorphous molybdenum oxide thin films with good photoelectric properties. The SHJ solar cells were fabricated making use of the HWOSD MoO_x as the HSL. Investigations and optimizations of the device structure, interface passivation and annealing process were carried out. A power conversion efficiency up to 21.10% was achieved for a champion SHJ solar cell with the structure of Ag/ITO/n-type a-Si:H/ intrinsic a-Si:H/n-type textured c-Si/intrinsic a-Si:H/MoO_x/Ag. Dark J-V-T characteristics were analysed to understand the transport mechanisms of the novel heterojunction solar cells.

2. Preparation of MoO_x thin films by novel HWOSD technique

A schematic diagram of the HWOSD technique is presented in Fig. 1. In a deposition chamber with oxygen atmosphere, molybdenum wires are electrically heated to a high temperature. MoO_x molecules are generated on the surface of the hot molybdenum wires and are sublimated directly into the chamber. The MoO_x molecules adsorb, diffuse, coalesce and finally form the MoO_x thin films on the substrate. During the deposition, the substrate temperature was lower than 70℃. The molybdenum wires with a purity of 99.995% and a diameter of 1 mm were used. The hot wire temperature, oxygen flow rate and deposition pressure were optimized to be 1095±5℃, 4 sccm and 0.2 Pa, respectively. Under the optimal condition, the deposition rate of the MoO_x thin films is about 9nm/min.

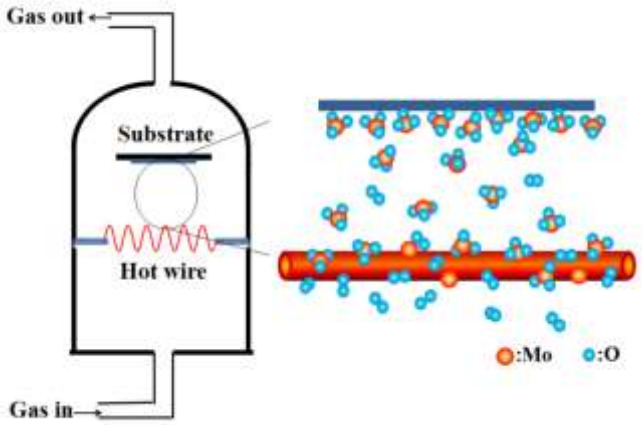

Fig.1 Schematic diagram of hot wire oxidation-sublimation deposition technique.

The novel HWOSD technique is attractive in many ways. Actually, it is somewhat similar to the well-known hot wire chemical vapor deposition technology [23]. Some of the advantages of this technique make it very easy to scale up for industrialization. Scaling to large areas merely requires an increase in number and/or length of molybdenum wires along with a proportionally larger supply of oxygen gas. The deposition rate of MoO_x film using HWOSD technique can be well adjusted by varying the oxygen pressure and/or the temperature of the molybdenum wires. Powder spattering, which is easy to occur during thermal evaporation[2-4], can be avoided. Next, conformal coating on any type of surface shape is possible for the HWOSD technique due to the gas-phase and surface diffusion of MoO_x molecules, which is conducive to the formation of good coverage on textured silicon substrates. Furthermore, the HWOSD technique is based on the characteristic of higher melting point of molybdenum and lower boiling point of molybdenum oxide. Therefore, it is suitable to be used to fabricate other metal oxides with similar characteristics, such as WO_x and VO_x.

3. Results and discussion

3.1 Characteristics of the MoO_x thin films prepared by HWOSD

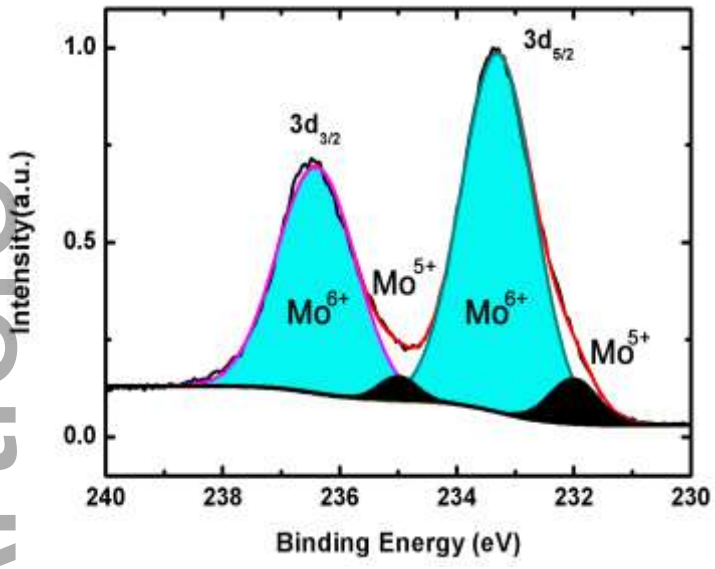

Fig. 2 The Mo 3d core level XPS spectrum for a MoO_x film fitted with multiple Voigt peaks (shaded areas) to quantify the contribution of different oxidation states.

During the process of hot wire oxidation-sublimation deposition, hot wire temperature and oxygen pressure are two important parameters affecting the opto-electronic properties of the deposited MoO_x thin films. Under the optimized hot wire temperature (1095±5℃) and oxygen pressure (0.2Pa), an average transmittance of 94.2% in the wavelength range of 400-1100 nm can be obtained on a 15nm MoO_x thin film. (The effect of the oxygen pressure on the transmittance of the MoO_x thin films is given in Figure S1). The dark conductivity of the optimized MoO_x film is 1.6×10^{-6} S/cm. The XRD spectrum shows that the HWOSD MoO_x thin film is in an amorphous structure (Figure S2).

Figure 2 shows the XPS spectrum of the Mo 3d core level in MoO_x thin film. The two major peaks, with binding energies of 233.3 eV and 236.4 eV, correspond to the Mo^{6+} $3d_{5/2}$ and $3d_{3/2}$, respectively[5, 19]. And the minor ones centered at 232.0 eV and 235.0 eV can be attributed to Mo^{5+}. The estimated O/Mo atomic ratio of the MoO_x thin film is about 2.94, which closes to the stoichiometric ratio of 3. The relatively high oxygen content in the MoO_x thin films usually leads to a high work function[18, 19] .

3.2 Surface morphologies and passivation effect of MoO_x on Si substrates

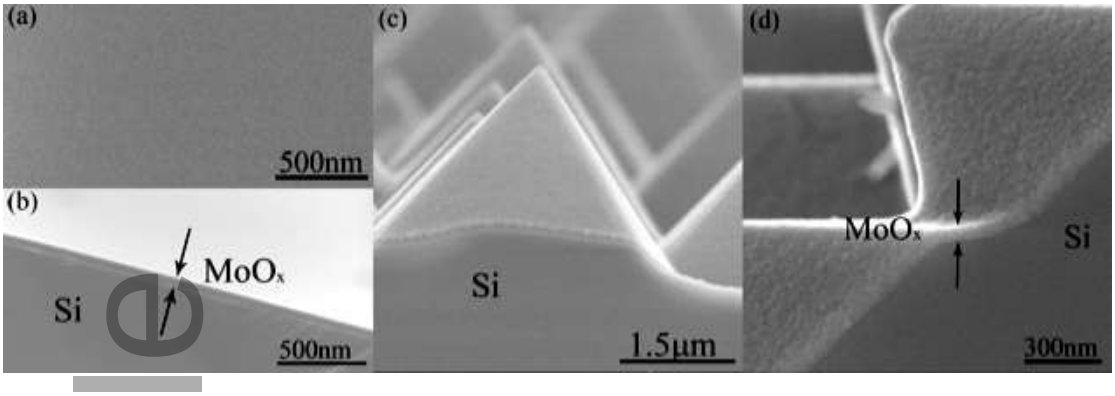

Fig. 3 (a) Top-view SEM image of MoO_x (25nm) on polished Si substrate. (b) Cross-sectional SEM image of MoO_x (70 nm) on polished Si substrate. (c, d) SEM images of MoO_x (70 nm) on textured Si wafers.

SEM images of the MoO_x thin films deposited on Si wafers are shown in Fig. 3. Figure 3 (a) and (b) exhibit the top-view and cross-sectional SEM images of the MoO_x films on polished Si substrates, respectively. It can be seem that compact MoO_x films with high thickness uniformity were formed on the polished Si substrates by using HWOSD. The SEM images of pyramid-shaped silicon surfaces covered with HWOSD MoO_x thin films are shown in Fig. 3 (c) and (d). Conformal coverage of the MoO_x thin films on the random pyramids is realized. The nice coverage characteristics can be confirmed by the elemental EDS mappings of O and Mo (Figure S3).

The effective lifetimes for n-type CZ Si wafers sandwiched between intrinsic a-Si:H (i a-Si:H) thin film or i a-Si:H/MoO_x combination layer as a function of excess carrier density were measured and compared (Figure S4). The i a-Si:H/MoO_x combination layer passivated sample shows enhanced lifetimes in the whole carrier injection concentration range of 7×10^{14} cm^{-3}~$1\times10^{16}$$cm^{-3}$ and a maximum lifetime up to 1.3 ms is achieved. The recombination current density (J_0) and the implied open circuit voltage (iV_{oc}) under one sun illumination are 26 fA/cm^2 and 697mV, respectively. The results demonstrate the effective field passivation effect of the molybdenum oxide film on the surface of c-Si. The high work function of the MoO_x layer produces a large band bending of the n-type c-Si surface and thus reduces the surface recombination effectively.

3.3 Optimization of the SHJ solar cells with MoO_x as HSL

The structure of the heterojunction solar cells with MoO_x HSL is shown in Fig. 4(a).

The illuminated side (front side) structure of the devices is set to be Ag grid/ITO/n-type a-Si:H/ i a-Si:H. The rear side structure is Ag/MoO_x/i a-Si:H. The main reason for putting the MoO_x HSL on the back side of the solar cell is to avoid the ITO layer sputtering and make the MoO_x contacting directly with Ag electrode. In this case, the deterioration of the MoO_x thin film related to the ITO sputtering process [2, 24] can be avoided and the role of the HWOSD MoO_x HSL on the performance of the SHJ solar cells can be well demonstrated. Of course, without the ITO layer, the SHJ solar cell fabrication process has become more concise. Another consideration is that, with this configuration, the novel solar cell can be compared with our reference SHJ devices. Generally, high-quality n-type a-Si:H thin films are easier to be realized than p-type a-Si:H. Therefore, using the n-type a-Si:H thin film in the front side of the SHJ solar cells is beneficial to achieve higher efficiency. The process flow chart for the fabrication of the novel and reference SHJ solar cells is illustrated in Fig.4 (b).

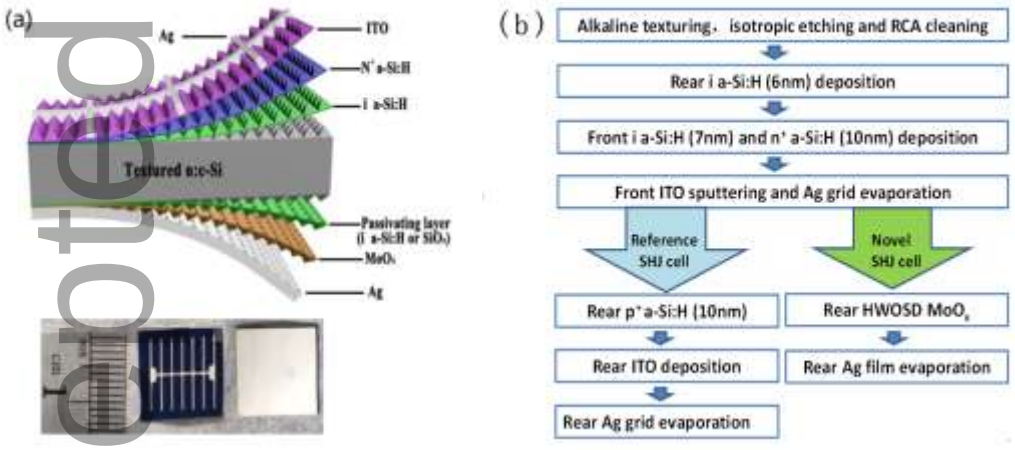

Fig. 4 (a) Cross-sectional schematic of the heterojunction solar cells with MoO_x HSL and photographs of the front and back of the HSL device.

(b) Process flow chart for the fabrication of the novel and reference SHJ solar cells.

Effective interface passivation plays critical role in increasing the performance of the SHJ solar cells. We found that the SHJ solar cells with MoO_x HSL directly deposited on Si substrates usually show much worse performance than a traditional SHJ solar cell, implying a serious recombination of photo-generated carriers at the MoO_x/c-Si interface. Different passivation layers, including intrinsic a-Si:H thin film, UV/O_3 photo-oxidized SiO_x, and the combination of a-Si:H and SiO_x, were adopted to

passivate the c-Si substrates before the deposition of MoO_x (Table S1). Compared with the solar cell without any passivation layer, all the passivation methods we tried improved the performances of the solar cells to some extent. Among them, the intrinsic a-Si:H layer deposited using PECVD exhibits the best passivation effect. The UV/O_3 treatment is quite simple compared with the a-Si:H deposition technique. However, the passivation effect of the UV/O_3 photo-oxidized SiO_x layer is less than satisfactory. Similar to reported in the literature[2], we also noticed that the SiO_x layer may lead to the deterioration of the annealing performance of a SHJ solar cell with MoO_x HSL, which will be discussed later. Therefore, we used the PECVD a-Si:H as the passivation layer at present stage.

Influence of the MoO_x HSL thickness (10nm-71nm) on the photovoltaic parameters of the SHJ solar cells was investigated (Figure S5). In the case that the thickness of the MoO_x HSL is too small (e.g. 10nm), the space charge region or the inversion layer near the c-Si surface may not be well formed, which is not favorable for the separation and collection of the photo-generated carriers. However, as for the condition of excessive MoO_x thickness (>14nm), the consequentially enhanced recombination in the MoO_x layer leads to the reduced carrier collection and then decline of the open circuit voltage (V_{oc}) and a rapid drop in the short circuit current density (J_{sc}). Despite the similar behavior as V_{oc} and J_{sc} under very small or very large thickness, the FF was kept to be at a relatively high value for the MoO_x thickness between 14nm-55nm due to the almost invariable series resistance. Considering all the photovoltaic parameters of the series of the SHJ solar cells, we determined an optimal MoO_x thickness of 14 nm. A power conversion efficiency of 18.11% was achieved for the SHJ solar cell with a 14 nm MoO_x as the HSL.

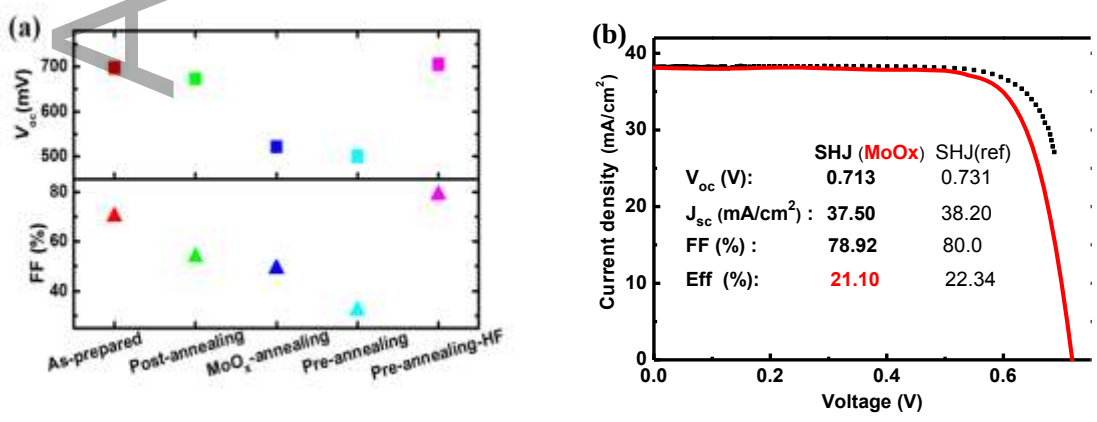

Fig. 5 (a) Influence of annealing process on V_{oc} and FF of the SHJ solar cells with MoO_x HSL. (b) Light J-V characteristics of a champion SHJ solar cell with MoO_x HSL (red line) and a reference SHJ solar cell (black dots).

Post-annealing as a low-temperature step with temperatures from 150°C to 350°C is a typical process needed for the fabrication of conventional SHJ solar cells, which can improve the overall performance of the devices. However, post-annealing tends to show a bad effect on the SHJ solar cells with metal oxides (such as MoO_x, WO_x, VO_x) as the hole selective transport layer[2, 6]. Many researches related to the degradation mechanism have been carried out. It was reported that the work functions of metal oxides and the characteristics of the interface between the metal oxides and the c-Si have been changed by post-annealing[25]. Stephanie Essig et al.[26] showed that effusion of hydrogen from the adjacent layers is a likely cause for the degradation for the SHJ solar cells with MoO_x HSL contacts. They suggested a pre-MoO_x-deposition annealing step to reduce the hydrogen content of the a-Si:H layer and allow high FF to be obtained. More research on the annealing process of SHJ solar cells with MoO_x HSL is still needed.

In this paper, an investigation on the annealing process of the SHJ solar cells with the MoO_x HSL was carried out and the influences of different annealing processes on the V_{oc} and FF of the SHJ solar cells are illustrated in Fig. 5 (a). As a reference, the V_{oc} and FF of an as-prepared SHJ solar cell without undergoing any annealing process are included as shown in red symbols. Similar to reported in the literature, annealing after the fabrication of the whole device (post-annealing, 190°C, 5min) leads to deterioration in device performance (green symbols). MoO_x-annealing (blue symbols) in Fig. 5 (a) refers to an annealing process that was carried out just after the preparation of MoO_x and before the deposition of silver electrode. V_{oc} and FF of the solar cell are further reduced with MoO_x-annealing compared with the post-annealing process, indicating serious damage to the exposed MoO_x layer was caused by the MoO_x-annealing process. In order to avoid the annealing damage to the MoO_x layer, annealing process was carried out before the preparation of the MoO_x layer, namely pre-annealing. The solar cell performance, disappointingly, is worse

instead of getting better. Possible reason is that an a-Si:H/SiO_x double-layer is formed during the pre-annealing process in the air atmosphere. Thus, dipoles could be formed at the SiO_x/MoO_x interface[27], which have a negative effect on the energy band bending and the selective transportation of the carriers. Therefore, we removed the oxidation layer on the amorphous silicon by HF solution (2%) treatment after the pre-annealing process and immediately prepared the MoO_x HSL and the metal back electrode to finish the device fabrication. Just as expected, the performance of the pre-annealing-HF sample shows a remarkable improvement as depicted in Fig. 5(a). The light J-V curve and PV parameters of a champion SHJ solar cell fabricated with the pre-annealing-HF process are shown in Fig. 5(b). An efficiency of 21.10% with V_{oc} of 713 mV, J_{sc} of 37.50 mA/cm^2 and FF of 78.92% was achieved for the SHJ solar cell with a MoO_x HSL. The integrated photocurrent density calculated from the external quantum efficiency is 37.2mA/cm^2 (Figure S6), which is in good agreement with the measured J_{sc}. For comparison, the J-V curve and PV parameters of an optimized reference SHJ solar cell(15.6×15.6 cm^2) are also given in Fig. 5(b). We can find that, at present stage, the performance of the novel SHJ solar cell is still lower than that of the reference SHJ solar cell. It should be noted that the novel SHJ solar cells are affected by the size effect of the solar cells. The size of the novel SHJ solar cells is about 1×1 cm^2. The edges of the device are not well passivated at present stage. If larger Si substrates were used, or if the edges of the devices were well passivated, higher performance can be expected for the SHJ solar cells.

The performance of the SHJ solar cells with the HWOSD MoO_x HSL is comparable to those of the SHJ solar cells with MoO_x HSL prepared by thermal evaporation[2, 4], electron-beam evaporation[15, 20] or atomic layer deposition[21]. The simplification and scalability of the MoO_x preparation and the simplified fabrication process of the devices with ITO free make the HWOSD MoO_x a great potential substitute for the doped Si layer in high efficiency c-Si solar cells in the future.

3.4 Transport mechanisms of the SHJ solar cells with HWOSD MoO_x HSL

Inspired by the great potential of the SHJ solar cells with MoO_x HSL, a lot of

researches, numerically or experimentally, on the current extraction of charge carriers via the MoO_x HSL were carried out to deeply understand the transport mechanisms and to assist the engineering of the novel SHJ solar cells[6, 28, 29]. It was shown that, for an effective hole extraction, a sufficiently high MoO_x work function or/and efficient trap-assisted tunneling paths are requirements have to be fulfilled [28, 29]. Based on the analysis of the dark *J-V-T* characteristics, transport mechanisms including trap-assisted tunnel of holes at low voltage and transport behavior of a Schottky-like junction at higher voltage were proposed by R. García-Hernansanza et al. for a SHJ solar cell with a thermally evaporated MoO_x HSL and without any passivation layer[6]. For our SHJ devices with a MoO_x HSL fabricated using HWOSD and with an a-Si:H passivation layer prepared by PECVD, fairly high V_{oc} of above 710 mV was achieved. It is necessary to investigate and understand the mechanisms governing charge carrier transport of the novel heterojunction and to further improve the performance of the devices.

Dark *J-V-T* measurements were carried out for a SHJ solar cell with the structure of Ag/ITO /n^+ a-Si:H /i a-Si:H/n c-Si/i a-Si:H/ MoO_x/Ag in a temperatures range of 200K to 380K and the dark *J-V* curves are shown in Fig. 6 (a). The corresponding photovoltaic parameters of the device are V_{oc}=710mV, FF=77.0%, J_{sc}=37.3mA/cm^2 and Eff=20.4%.

Considering the change of the slopes of the *J-V* curves, two-diode model can be used to fit the experimental results [30]. The current density varied with the applied voltage can be written as:

$$J = J_{01}\left[e^{A_1(V-JR_s)} - 1\right] + J_{02}\left[e^{A_2(V-JR_s)} - 1\right] + \frac{V-JR_s}{R_{sh}} \qquad (1)$$

where J_{01} and J_{02} are the saturation current densities of diode 1 and 2, R_s and R_{sh} are the series and shunt resistance, A_1 and A_2 depend on the transport mechanisms. The contributions of diodes 1 and 2 to the *J-V* curves are generally considered to be in the high (>0.5V) and low (<0.5V) voltage regions, respectively. The exponential factor A_i (i=1,2) generally has an empirical expression of $A_i=q/n_ikT$, where q is the electron charge, n_i the diode ideality factor, k the Boltzmann's constant, and T the absolute temperature.

Based on equation (1), the dark *J-V* curves were fitted. It was found that A_1 changes linearly with the increasing of $1/kT$ and a constant ideality factor n_1=1.2 can

be determined for the diode 1, which is often observed in a rectifier junction. However, A_2 does not change significantly in the whole experimental temperature range and no unified ideality factor n_2 can be determined. For a relatively narrow temperature region of $250K<T<330K$ ($35.0<1/kT<46.2$), fairly large diode ideality factor values varied between 3.51 and 3.93 can be obtained. In the traditional SHJ solar cells, large n_2 is usually considered to be a signal of serious shunt leakage current[31] or interface recombination[32] which certainly degrades the fill factor, V_{oc} and efficiency. In this work, the contradiction between the large n_2 and quite high V_{oc} and fill factor of the device implies different transport mechanisms from the traditional ones. Numerical calculation has shown that the trap-assisted tunnel transport plays an important role in the current extraction of the novel SHJ solar cells [28], which has been proved by R. García-Hernansanza et al in a MoO_x/n c-Si heterojunction device[12]. According to the large value and the temperature dependence characteristic of n_2, trap-assisted tunnel transport at lower voltage range is also considered for our novel SHJ solar cell and will be discussed further.

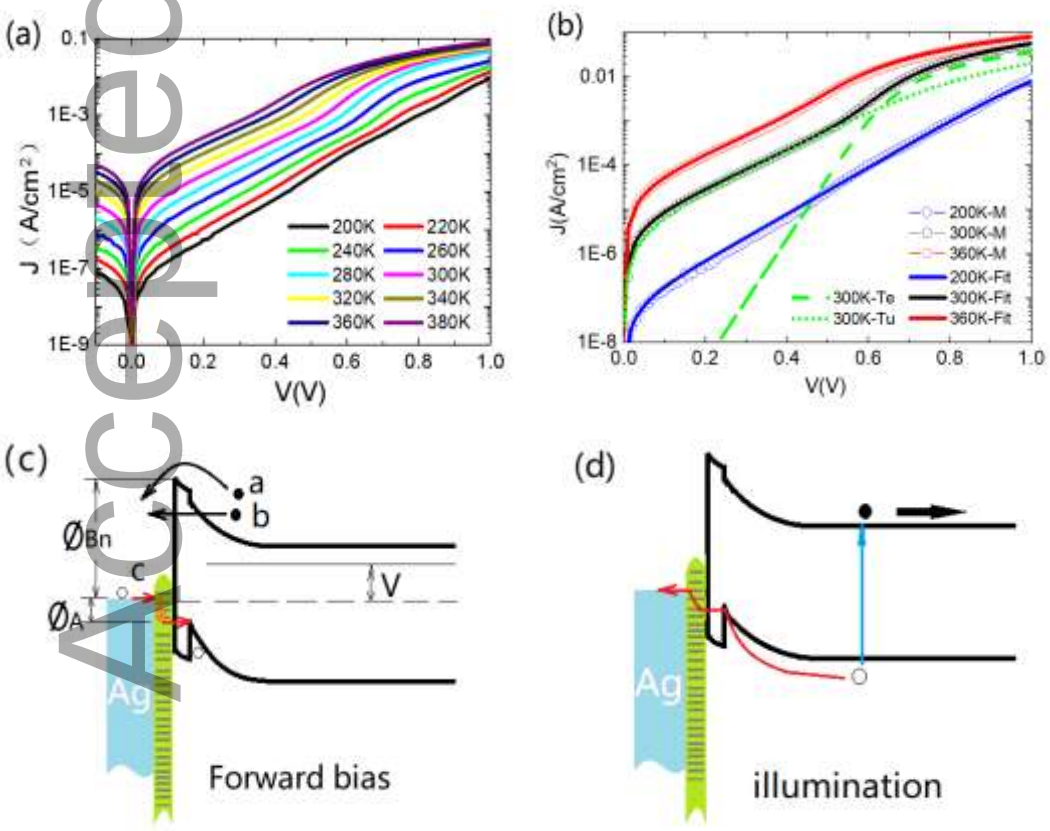

Fig. 6 (a) Dark *J-V* curves of a novel SHJ solar cell measured at the temperatures from 200K to 380K. (b) Experimental (hollow symbols) and fitting (solid lines) dark *J-V* curves under forward bias for the novel SHJ solar cell under three temperatures of

200K, 300K and 360K. The green dashed and dotted lines respectively represent the fitted J_{Te} (majority-carrier processes a and b) and J_{Tu} (minority-carrier process c) for the *J-V* curve measured under 300K. (c) Schematic energy band structures of the MoOx/i a-Si:H/n c-Si heterocontact under forward bias. Three transport processes, including thermionic emission of electrons, thermal assisted tunneling of electrons and tunneling of holes are denoted by a, b, and c, respectively. (d) Schematic energy band structures of the heterocontact under illumination.

Considering the high work function (>6eV) and high density of gap states characteristics of amorphous MoO_x[4], it is appropriate to think of the MoO_x/i a-Si:H/n c-Si heterocontact as a Schottky-like rectifier junction with large barrier height[12], whose energy band structures under forward bias and illumination are depicted in Fig. 6 (c and d). Based on the above analysis, three main transport processes, including thermionic emission of electrons, thermal assisted tunneling of electrons and trap-assisted tunneling of holes, denoted by a, b, and c respectively, are considered as the basic transport processes.

In both a and b processes, thermionic activation of majority carriers is involved. Therefore, we use a total majority-carrier (electron) thermionic current density J_{Te} to represent the thermionic emission and thermal assisted tunneling processes. In the process c, minority carriers (holes) tunnel through the gap states of the MoO_x layer into the top of the valence band (TVB) of the c-Si and then recombine with electrons. J_{Tu} is used to express the current density related to the trap-assisted tunneling of holes. Now, the equation (1) can be expressed as:

$$J = J_{Te} + J_{Tu} + J_{shunt}$$

$$= J_{01}[\exp(\frac{q(V - JR_s)}{n_1 kT}) - 1] + J_{02}[\exp(\frac{q(V - JR_s)}{E_0}) - 1] + \frac{V - JR_s}{R_{sh}} \quad (2)$$

$$J_{01} = C(T)\exp\left(-\frac{q\phi_{Bn}}{kT}\right) \quad (3)$$

$$J_{02} = B(T)\exp\left(-\frac{q\phi_A}{kT}\right) \quad (4)$$

where $q\phi_{Bn}$ is the effective barrier height for electrons, C(T) a temperature dependent pre-factor, E_0 the tunneling barrier energy and $q\phi_A$ the activation energy of holes. E_0 is related to the almost invariable slopes of the dark *J-V* curves at low bias as

Fig. 6 (a) shows and is simplified to be a constant in the following fittings. $q\phi_A$ is actually the difference between the top of the valence band (TVB) of c-Si surface and the Fermi lever of the Ag electrode, as shown in Fig. 6(c). Comparing the equations (1) and (2), we can easily find that J_{Te} and J_{Tu} correspond to the contributions of diode 1 and 2, respectively. In the equation (2), the transport mechanisms corresponding to the two diodes are specified.

Three forward *J-V* curves measured at temperatures of 200K, 300K, and 360K were fitted according to equation (2), as shown in Fig. 6 (b). Good agreement between the measured and the fitted curves in the whole voltage range can be obtained. The fitting results for E_0, $q\phi_A$, and $q\phi_{Bn}$ are 0.087eV, 0.29eV, and 0.98eV, respectively. To better understand the respective contributions of J_{Tu} and J_{Te} to the total J-V curve, the fitted J_{Te} and J_{Tu} for the *J-V* curve measured under 300K, as an example, are depicted in dashed and dotted lines in Fig. 6 (b).

It can be seen that J_{Te} starts to play a major role as V>0.6V. As we known, the dominate transport mechanism at high bias plays an important role in the performance, especially V_{oc}, of the solar cells. Therefore, the high V_{oc} of the novel SHJ solar cells should be related to the large effective barrier height $q\phi_{Bn}$ of the transport processes a and b. In this case, a strong inversion of the energy band near the n-type c-Si surface is formed and effective collection of photo-generated electrons can be achieved, as shown in Fig. 6 (d). The $q\phi_{Bn}$ we obtained is a little bit higher than that reported by R. García-Hernansanza et al.[6], which coincides with the fact that the V_{oc} of our device is higher. It is worth noting that the fitted $q\phi_{Bn}$ is much smaller than the work-function difference between the MoO_x and n type c-Si. The electrostatic potential and the barrier height can be modified by the interface-trapped charges and also the possible dipoles [33]. If the interface was better passivated, larger barrier height could be expected. Furthermore, as a type of inversion layer solar cells[34], the high conductivity of the inversion layer may lead to good transverse transportation and then high FF can be achieved.

In the case of lower forward bias (V<0.5V), the tunnel current density J_{Tu} dominates the *J-V* curve and causes a lower slope of Log (J) versus V. The high defect density in the band gap of amorphous MoO_x makes the tunneling process easily and the minority current density J_{Tu} is larger than that of a typical metal/Si Schottky junction. This tunneling channel is critical important for the carriers collection under

illumination. Photo-generated holes can be effectively collected through this tunneling channel, which is beneficial to achieve high open-circuit voltage. In addition, we can also see from the Fig. 6 (b) that, in the high voltage region, the contribution of the minority current density J_{Tu} should not be ignored like a typical majority-carrier device. The high barrier or the strong inversion characteristic makes the Schottky-like junction a high minority-carrier injection ratio.

4. Conclusions

The hot wire oxidation-sublimation deposition method is demonstrated to be a promising technique for preparation of high-quality MoO_x films with uniform thickness, compact structure, nice photoelectric properties and conformal coverage on textured Si substrates. Novel silicon heterojunction solar cells with the HWOSD MoO_x thin films as the HSL were successfully fabricated. An efficiency of 21.10% was achieved for the champion SHJ solar cell with a MoO_x HSL fabricated by the scalable HWOSD technique.

Analysis of the dark *J-V-T* characteristics shows that tunneling of holes through the gap states of the MoO_x layer causes the low slope of the plot of Log (*J*) versus *V* at low voltage range (V<0.5V). This tunneling channel is beneficial for the holes collection under illumination. A high Schottky-like barrier can be obtained from the fitting of the J-V curve in the high voltage range (>0.6), which indicates a strong inversion of the c-Si energy band near the interface. The high effective barrier and the strong inversion layer promote the efficient collection of the photo-generated carriers and lead to good transverse transportation, which are helpful for achieving high V_{oc} and FF. It is this characteristic that makes the novel MoO_x/c-Si heterojunction solar cells inherently possess potential of high efficiency. More research work is needed to fully reveal the potential of the novel SHJ solar cells.

5. Experimental details

5.1 Fabrication of silicon heterojunction solar cells

N-type <100> float zone (FZ) silicon wafers with a thickness of 250 μm and a resistivity of 1 to 5 Ω·cm were used as the substrates. Alkaline texturing and isotropic etching were carried out in succession to form random pyramids with less sharp tops on both sides of the c-Si wafers. After texturing, the c-Si substrates were chemically

cleaned according to the standard RCA procedure. Before proceeding to the next step, the textured silicon wafers were dipped in 2% hydrofluoric acid for 1 min to remove the surface oxide layer.

The illuminated side **(**front side**)** structure of the devices is set to be Ag grid/ITO/n-type a-Si:H/ i a-Si:H. Intrinsic (~7 nm) and n-type (~10 nm) a-Si:H as the passivation and the electron selective transport layer were successively deposited on one side of the c-Si substrates by means of plasma enhanced chemical vapor deposition (PECVD) under a substrate temperature of about 200 $^{\circ}$C. The front electrode consists of an indium tin oxide layer (ITO 80nm) by magnetron sputtering and a silver grid by thermal evaporation. The rear side structure of the SHJ solar cells is Ag/MoO_x/i a-Si:H. The i a-Si:H thin film (~6nm) deposited by PECVD was also used for interface passivation. The MoO_x thin film, as the HSL to replace the traditional p-type a-Si:H, was prepared by hot wire oxidation-sublimation deposition. Thermal evaporated Ag film was used as the rear electrode. The active area of the devices is 1 cm^2.

5.2 Characterization of thin films and devices

Thicknesses of MoO_x and ITO thin films were measured using a surface profilometer (ERUKER-DektakXT). Surface morphologies and elemental analysis of the MoO_x thin films deposited on c-Si wafers were characterized using scanning electron microscope (SEM, Hitachi SU8010) and energy dispersive spectrometer (EDS, Bruker 6-30). Elemental compositions of the MoO_x films were characterized using X-ray photoelectron spectroscopy (XPS, Thermo Scientific ESCALAB250Xi) under ultra-high vacuum ($<2\times10^{-9}$ mbar). Minority carrier lifetimes of the passivated c-Si wafers were evaluated using the quasi-steady-state photo conductance (QSSPC Sinton WCT-120). Light current density-voltage (*J-V*) curves of the solar cells were obtained under AM1.5 (100 mW/cm^2, 25℃) illumination. Dark *J-V-T* characteristics of the SHJ solar cells were measured at the temperatures from 200K to 380K.

Acknowledgements

This work was supported by the National Key R&D Program of China (2018YFB1500102) and the National Natural Science Foundation of China (No.61604153 and No.61674150). Support from the Sino-Danish Center for Education and Research (SDC) is fully acknowledged.

References

[1] P. Q. Gao, Z. H. Yang, J. He, J. Yu, P. P. Liu, J. Y. Zhu, Z. Y. Ge, J. C. Ye, Adv. Sci. 2018, 5, 20; X. B. Yang, E. Aydin, H. Xu, J. X. Kang, M. Hedhili, W. Z. Liu, Y. M. Wan, J. Peng, C. Samundsett, A. Cuevas, S. De Wolf, Adv. Energy Mater. **2018**, 8, 7; Z. Wang, P. Li, Z. Liu, J. Fan, X. Qian, J. He, S. Peng, D. He, M. Li, and P. Gao, APL Materials, **2019**, 7, 110701.

[2] J. Geissbuhler, J. Werner, S. M. de Nicolas, L. Barraud, A. Hessler-Wyser, M. Despeisse, S. Nicolay, A. Tomasi, B. Niesen, S. De Wolf, C. Ballif, Appl. Phys. Lett. **2015**, 107, 5.

[3] J. Bullock, M. Hettick, J. Geissbuhler, A. J. Ong, T. Allen, C. M. Sutter-Fella, T. Chen, H. Ota, E. W. Schaler, S. De Wolf, C. Ballif, A. Cuevas, A. Javey, Nat. Energy **2016**, 1, 7.

[4] C. Battaglia, X. T. Yin, M. Zheng, I. D. Sharp, T. Chen, S. McDonnell, A. Azcatl, C. Carraro, B. W. Ma, R. Maboudian, R. M. Wallace, A. Javey, Nano Lett. **2014**, 14, 967; J. Wang, H. Lin, Z. Wang, W. Shen, J. Ye, P. Gao, Nano Energy, **2019**, 66, 104116.

[5] J. N. Tong, Y. M. Wan, J. Cui, S. Lim, N. Song, A. Lennon, Appl. Surf. Sci. **2017**, 423, 139.

[6] R. Garcia-Hernansanz, E. Garcia-Hemme, D. Montero, J. Olea, A. del Prado, I. Martil, C. Voz, L. G. Gerling, J. Puigdollers, R. Alcubilla, Sol. Energy Mater. Sol. Cells **2018**, 185, 61.

[7] O. Almora, L. G. Gerling, C. Voz, R. Alcubilla, J. Puigdollers, G. Garcia-Belmonte, Sol. Energy Mater. Sol. Cells 2017, 168, 221; W. L. Wu, J. Bao, X. G. Jia, Z. T. Liu, L. Cai, B. H. Liu, J. W. Song, H. Shen, Phys. Status Solidi-Rapid Res. Lett. **2016**, 10, 662; G. Masmitja, L. G. Gerling, P. Ortega, J. Puigdollers, I. Martin, C. Voz, R. Alcubilla, J. Mater. Chem. A **2017**, 5, 9182.

[8] M. Mews, L. Korte, B. Rech, Sol. Energy Mater. Sol. Cells 2016, 158, 77; M. Mews, A. Lemaire, L. Korte, IEEE J. Photovolt. **2017**, 7, 1209.

[9] M. Y. Xue, R. Islam, Y. S. Chen, J. Y. Chen, C. Y. Lu, A. M. Pleus, C. Tae, K. Xu, Y. Liu, T. I. Kamins, K. C. Saraswat, J. S. Harris, J. Appl. Phys. **2018**, 123, 5.

[10] H. Imran, T. M. Abdolkader, N. Z. Butt, IEEE Trans. Electron Devices **2016**, 63, 3584.

[11] P. Ravindra, R. Mukherjee, S. Avasthi, IEEE J. Photovolt. **2017**, 7, 1278.

[12] L. G. Gerling, S. Mahato, A. Morales-Vilches, G. Masmitja, P. Ortega, C. Voz, R. Alcubilla, J. Puigdollers, Sol. Energy Mater. Sol. Cells **2016**, 145, 109.

[13] S. Avasthi, W. E. McClain, G. Man, A. Kahn, J. Schwartz, J. C. Sturm, Appl. Phys. Lett. **2013**, 102, 4; M. M. Plakhotnyuk, N. Schuler, E. Shkodin, R. A. Vijayan, S. Masilamani, M. Varadharajaperumal, A. Crovetto, O. Hansen, Jpn. J. Appl. Phys. **2017**, 56, 8.

[14] H. Tong, Z. H. Yang, X. X. Wang, Z. L. Liu, Z. X. Chen, X. X. Ke, M. L. Sui, J. Tang, T. B. Yu, Z. Y. Ge, Y. H. Zeng, P. Q. Gao, J. C. Ye, Adv. Energy Mater. **2018**, 8,

10.
[15]J. Yu, Y. M. Fu, L. Q. Zhu, Z. H. Yang, X. Yang, L. Ding, Y. H. Zeng, B. J. Yan, J. Tang, P. Q. Gao, J. C. Ye, Sol. Energy **2018**, 159, 704.
[16]P. P. Boix, J. Ajuria, I. Etxebarria, R. Pacios, G. Garcia-Belmonte, J. Bisquert, J. Phys. Chem. Lett. **2011**, 2, 407; W. Y. Zhang, Q. L. Meng, B. X. Lin, Z. X. Fu, Sol. Energy Mater. Sol. Cells **2008**, 92, 949.
[17]J. Meyer, S. Hamwi, M. Kroger, W. Kowalsky, T. Riedl, A. Kahn, Adv. Mater. **2012**, 24, 5408; Y. Z. Guo, J. Robertson, Appl. Phys. Lett. **2014**, 105, 4; C. Battaglia, S. M. de Nicolas, S. De Wolf, X. T. Yin, M. Zheng, C. Ballif, A. Javey, Appl. Phys. Lett. **2014**, 104, 5.
[18]M. T. Greiner, L. Chai, M. G. Helander, W. M. Tang, Z. H. Lu, Adv. Funct. Mater. **2012**, 22, 4557.
[19]B. C. Han, M. Gao, Y. Z. Wan, Y. Li, W. L. Song, Z. Q. Ma, Mater. Sci. Semicond. Process **2018**, 75, 166.
[20]R. Sivakumar, R. Gopalakrishnan, M. Jayachandran, C. Sanjeeviraja, Curr. Appl. Phys. **2007**, 7, 51.
[21]B. Macco, M. F. J. Vos, N. F. W. Thissen, A. A. Bol, W. M. M. Kessels, Phys. Status Solidi-Rapid Res. Lett. **2015**, 9, 393; J. Ziegler, M. Mews, K. Kaufmann, T. Schneider, A. N. Sprafke, L. Korte, R. B. Wehrspohn, Appl. Phys. A-Mater. Sci. Process. **2015**, 120, 811.
[22]S. H. Mohamed, S. Venkataraj, Vacuum **2007,** 81, 636; J. M. Pachlhofer, C. Jachs, R. Franz, E. Franzke, H. Kostenbauer, J. Winkler, C. Mitterer, Vacuum **2016**, 131, 246.
[23]R. E. I. Schropp, Thin Solid Films **2015**, 595, 272.
[24]D. Sacchetto, Q. Jeangros, G. Christmann, L. Barraud, A. Descoeudres, J. Geissbuhler, M. Despeisse, A. Hessler-Wyser, S. Nicolay, C. Ballif, IEEE J. Photovolt. **2017**, 7, 1584.
[25]T. Zhang, C. Y. Lee, Y. M. Wan, S. Lim, B. Hoex, J. Appl. Phys. **2018**, 124, 7.
[26]S. Essig, J. Dreon, E. Rucavado, M. Mews, T. Koida, M. Boccard, J. Werner, J. Geissbuhler, P. Loper, M. Morales-Masis, L. Korte, S. De Wolf, C. Ballif, Sol. RRL (Germany) **2018**, 2, 1700227 (5 pp.).
[27]K. Kita, A. Toriumi, Appl. Phys. Lett. **2009**, 94, 3.
[28]C. Messmer, M. Bivour, J. Schon, M. Hermle, J. Appl. Phys. **2018**, 124, 8.
[29]R. A. Vijayan, S. Essig, S. De Wolf, B. G. Ramanathan, P. Loper, C. Ballif, M. Varadharajaperumal, IEEE J. Photovolt. **2018**, 8, 473.
[30]R. Hussein, D. Borchert, G. Grabosch, W. R. Fahrner, Sol. Energy Mater. Sol. Cells **2001**, 69, 123.
[31]S. Dongaonkar, J. D. Servaites, G. M. Ford, S. Loser, J. Moore, R. M. Gelfand, H. Mohseni, H. W. Hillhouse, R. Agrawal, M. A. Ratner, T. J. Marks, M. S. Lundstrom, M. A. Alam, J. Appl. Phys. **2010**, 108.
[32]R. V. K. Chavali, J. R. Wilcox, B. Ray, J. L. Gray, M. A. Alam, IEEE J. Photovolt. **2014,** 4, 763.
[33] L. G. Gerling, S. Mahato, A. Morales-Vilches, G. Masmitja, P. Ortega, C. Voz, R. Alcubilla, J. Puigdollers, Sol. Energy Mater. Sol. Cells, **2016**, 145, 109-115

[34] R. Har-Lavan, D. Cahen, IEEE J. Photovolt. **2013**, 3, 1443.

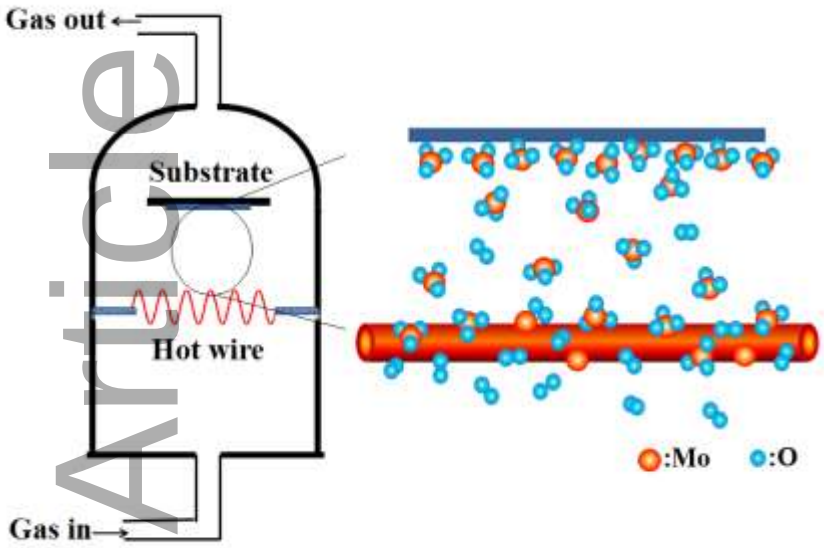

a hot wire oxidation-sublimation deposition (HWOSD) technique was developed to prepare molybdenum oxide thin films. Silicon heterojunction solar cells with the HWOSD MoO_x as a hole selective transport layer were fabricated. A power conversion efficiency up to 21.10% was achieved on a champion solar cell.